Biochimie 145 (2018) 137–144

Contents lists available at ScienceDirect

Biochimie

journal homepage: www.elsevier.com/locate/biochi

Research paper

Development of a thermal-stable structure-switching cocaine-binding aptamer

Aron A. Shoara, Oren Reinstein, Okty Abbasi Borhani, Taylor R. Martin, Sladjana Slavkovic, Zachary R. Churcher, Philip E. Johnson*

Department of Chemistry and Centre for Research on Biomolecular Interactions, York University, Toronto, Ontario, M3J 1P3, Canada

ARTICLE INFO

Article history:
Received 23 June 2017
Accepted 18 August 2017
Available online 21 August 2017

Keywords:
Aptamer design
DNA melts
NMR spectroscopy
Fluorescence spectroscopy
Isothermal titration calorimetry
DNA-Small molecule interactions

ABSTRACT

We have developed a new cocaine-binding aptamer variant that has a significantly higher melt temperature when bound to a ligand than the currently used sequence. Retained in this new construct is the ligand-induced structure-switching binding mechanism that is important in biosensing applications of the cocaine-binding aptamer. Isothermal titration calorimetry methods show that the binding affinity of this new sequence is slightly tighter than the existing cocaine-binding aptamer. The improved thermal performance, a T_m increase of 4 °C for the cocaine-bound aptamer and 9 °C for the quinine-bound aptamer, was achieved by optimizing the DNA sequence in stem 2 of the aptamer to have the highest stability based on the nearest neighbor thermodynamic parameters and confirmed by UV and fluorescence spectroscopy. The sequences in stem 1 and stem 3 were unchanged in order to retain the structure switching and ligand binding functions. The more favorable thermal stability characteristics of the OR3 aptamer should make it a useful construct for sensing applications employing the cocaine-binding aptamer system.

1. Introduction

The cocaine-binding aptamer has become a model system for the development of aptamer-based biosensors. The secondary structure of the aptamer is composed of three stems arranged into a three-way junction with both tandem AG base pairs and a dinucleotide bulge located at or adjacent to the three-way junction (Fig. 1) [1]. When stem 1 is six base pairs long, the aptamer folds in the free state and retains the same secondary structure when ligand-bound [1]. However, if stem 1 is shortened to be three base pairs in length, as shown in Fig. 1, the aptamer undergoes a ligand-induced structure switching binding mechanism. In the ligand-free state, the short stem 1 aptamer is loosely or poorly structured. Upon ligand binding, the aptamer folds or dynamically tightens into the secondary structure shown in Fig. 1 [1–5]. It is this structure-switching binding mechanism that has been exploited in many of the applications of the cocaine-binding aptamer in biosensor development, and consequently, the short stem 1 version of the cocaine-binding aptamer is a widely utilized version of the cocaine-binding aptamer [2,6–22].

The structure switching nature of the short stem 1 construct of the cocaine-binding aptamer must arise from the interplay between the destabilising reduction in the length of stem 1 and the stabilizing nature of ligand binding. This is demonstrated by the observation that tighter binding ligands for the cocaine-binding aptamer such as quinine [4,23,24], result in aptamer-ligand pairings with a higher melt temperature than the cocaine-bound aptamer [25]. Additionally, the steroid-binding aptamer, a three-way junction aptamer based on the cocaine-binding aptamer sequence, binds deoxycholic acid very weakly. This interaction is not tight enough to fold the version of the aptamer that contains a three-base-pair-long stem 1. Instead, deoxycholic acid binds and folds a version of this aptamer with a stem 1 four base pairs long [26].

Despite the widespread adoption of the short stem 1 version of the cocaine-binding aptamer (Fig. 1; MN19) in biotechnology, this sequence is not optimal, as it is only marginally stable at room temperature. This is demonstrated by our published temperature-dependent NMR studies [1], temperature-dependent ITC-based

* Corresponding author. Department of Chemistry, York University, 4700 Keele St., Toronto, Ontario, M3J 1P3, Canada.
E-mail address: pjohnson@yorku.ca (P.E. Johnson).

http://dx.doi.org/10.1016/j.biochi.2017.08.010
0300-9084/

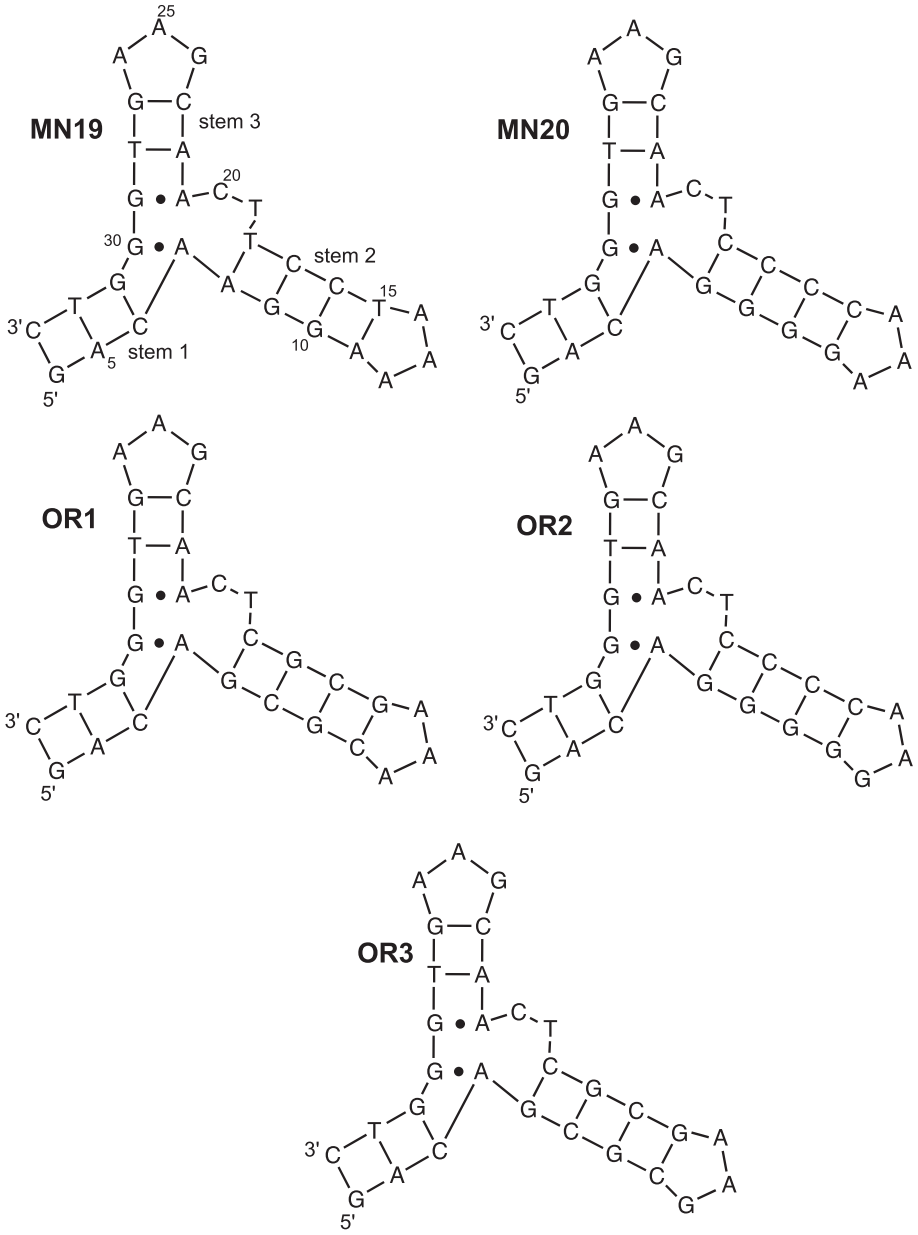

Fig. 1. Sequence and secondary structures of aptamers used in this study. For ease of comparison the numbering system is the same as used for the 36-nucleotide version of the aptamer and starts at 4 for these constructs.

binding studies [1,4], and DSC analysis [25]. The goal of this study is to develop a more thermally stable version of the cocaine-binding aptamer that preserves the functionally important ligand-induced structure-switching binding mechanism. To achieve this, we retained the three base pair-long stem 1 and the sequence of stem 3, as these stems are important for the structure-switching and ligand binding functions. We modify the sequence of stem 2 to obtain a cocaine-binding aptamer variant with as high a melt temperature as possible. We demonstrate that the resulting sequence, OR3 (Fig. 1), has these characteristics.

2. Materials and methods

2.1. Materials

DNA was obtained from Integrated DNA Technologies (IDT). DNA aptamer samples were dissolved in distilled deionized H_2O (ddH_2O) and then exchanged three times using a 3-kDa molecular weight cut-off concentrator with sterilized 1 M NaCl followed by three exchanges into ddH_2O. Aptamer samples were heated in a boiling water bath for 3 min and cooled in an ice bath prior to use to allow the DNA aptamer to anneal. Final aptamer and ligand concentrations were determined by UV–Vis spectroscopy using the extinction coefficients provided by suppliers.

2.2. Isothermal titration calorimetry

Isothermal titration calorimetry (ITC) experiments were performed using a MicroCal VP-ITC instrument. Samples were degassed at 4 °C for 5 min prior to use with the MicroCal Thermo Vac unit. All experiments were corrected for the heat of dilution of the titrant. Cocaine binding experiments were performed at low-c

conditions [27] using 20 μM aptamer solutions with a cocaine concentration of 3.6 mM at 20 °C in 140 mM NaCl, 20 mM TRIS buffer (pH 7.4), 5 mM KCl. Quinine binding experiments were performed for OR3 and MN19 in the presence of 140 mM NaCl (high salt) and with 0 mM NaCl (low salt) in 20 mM TRIS buffer (pH 7.4) with 40–80 μM aptamer solutions with a quinine concentration of 0.624–1.248 mM at 15 and 20 °C. All titrations were performed with the aptamer in the cell and ligand in the injector. Standard binding experiments consisted of 35 successive 8 μL injections spaced every 300 s, where the first injection was 2 μL. Data obtained at high salt conditions were analysed using the accompanying Origin 7.0 software fitting to a one-site binding model. Data obtained at low salt conditions were fit to a two-independent sites binding model [28,29]. The fitting of the two-site binding data was performed using the Matlab 14 software package.

2.3. UV melts

UV thermal melt experiments were performed using a Cary 100 spectrometer and 10-mm fused quartz cuvettes. The temperature was monitored throughout each experiment at 1 °C/min using a Cary Peltier controller. The DNA melting curves were observed in a temperature range of 5 °C–65 °C for cocaine-aptamer experiments, and 5 °C–80 °C for quinine-aptamer assays, as cocaine is more thermolabile than quinine [25,30]. Each experiment was performed in 20 mM sodium phosphate buffer (pH 7.4), 140 mM NaCl. For each ligand-aptamer complex, a concentration of aptamer was chosen to yield ~0.5 absorbance arbitrary units (a. u.) at 260 nm using the known extinction coefficients of the aptamer. Then, the ligand to aptamer molar ratio was kept constant at 95% ligand-bound based on the known K_d values [1,4]. The observed UV light absorbance at 260 nm from 4 to 6 replicates were averaged. Then the difference between the average bound and average free ligand absorbance was obtained. This difference was then normalized as $(\Delta I_{max} - \Delta I_i)/(\Delta I_{max} - \Delta I_{min})$ where ΔI_{max} is the maximum value of the difference between the bound and free ligand absorbance, ΔI_{min} is the minimum value of the difference between the bound and free ligand absorbance and ΔI_i is the value of the difference between the bound and free ligand absorbance at a particular temperature. Then the normalized absorbance was plotted against the temperature. To quantify the thermal shift, the first derivative of each thermal curve was plotted as a function of temperature.

2.4. Fluorescence spectroscopy

Fluorescence thermal shift assays were performed employing a 90°-light path Cary Eclipse spectrofluorometer and 10-mm fused quartz cuvettes. The temperature was monitored throughout each experiment at 1 °C/min using a Cary Peltier controller. The thermal shifts were observed in a temperature range of 5 °C–65 °C for cocaine-aptamer experiments and 5 °C–80 °C for quinine-aptamer assays. Each experiment was performed in 20 mM sodium phosphate buffer (pH 7.4), 140 mM NaCl. Ligand-aptamer complexes were optimized for the excitation and emission maxima of the corresponding ligand, photomultiplier tube (PMT) voltage, signal-to-noise ratio (SNR) and spectral bandwidth (SBW) parameters. For each ligand-aptamer complex, a ligand to aptamer molar ratio was chosen to ensure the aptamer was 95% ligand-bound based on the known K_d values [1,4]. The observed fluorescence emission intensities from 4 to 6 replicates were corrected for the inner-filter effect to compensate for the loss of the light intensity by the aptamer [31,32]. The obtained fluorescence intensities were averaged. Then the difference between the average bound and average free ligand fluorescence intensity was obtained. This difference was then normalized as $(\Delta I_i - \Delta I_{start})/(\Delta I_{end} - \Delta I_{start})$ where ΔI_{start} is the value of the difference between the fluorescence intensity of the ligand/aptamer mixture and free ligand fluorescence intensity at the start of the melt (lowest temperature), ΔI_{end} is the value of the difference between the fluorescence intensity of the ligand/aptamer mixture and free ligand fluorescence intensity at the end of the melt (highest temperature), and ΔI_i is the value of the difference between the fluorescence intensity of the ligand/aptamer mixture and free ligand fluorescence intensity at a particular temperature. The normalized fluorescence was then plotted against temperature. To quantify the thermal shift, the first derivative of each thermal curve was plotted as a function of temperature [33–36]. In the assays of the quinine-aptamer complexes, quinine was excited at 234 nm, and the emission maxima were recorded at 383 nm. For the assays of the cocaine-aptamer complexes, cocaine was excited at 232 nm, and the maximum fluorescence intensity was detected at 320 nm.

2.5. NMR analysis

1D ^{1}H NMR experiments on aptamer samples were performed using a 600 MHz Bruker Avance spectrometer in $H_2O/^2H_2O$ (90%/10%) at 5 °C. These sample conditions were chosen to result in spectra showing the sharpest signals and are identical to our previous studies [1,4,37]. Water suppression was achieved through the use of the WATERGATE sequence [38]. Aptamer concentration for NMR studies ranged from 0.3 to 0.5 mM.

3. Results

3.1. Aptamer thermal stability analysis

The thermal stability of the different stem 2 variants both free and bound to quinine was analysed by UV melting experiments. All the constructs displayed no evidence of being folded in the free state as their A_{260} versus temperature plots displayed a straight line with no sign of a typical sigmoidal denaturation curve (Fig. 2). In the presence of quinine, all the constructs exhibited a sigmoidal melt curve as shown for MN19•quinine and OR3•quinine in Fig. 2. From a first derivative analysis, the T_m values for the aptamer-quinine complexes were obtained and are listed in Table 1. These data show that the MN19-quinine complex has the lowest T_m value (35.5 ± 0.3 °C) and OR3 has the highest T_m value (44.2 ± 0.1 °C).

As a comparison for the UV melt analysis, the stability of MN19 and OR3 were also analysed using a fluorescence thermal shift assay based on the differential scanning fluorimetry technique [33]. This method is very sensitive, and the effects of both quinine and cocaine binding on the stability of MN19 and OR3 were analysed. When the aptamer binds its ligand, quinine and cocaine fluorescence intensity is quenched [39]. In this assay, the increase in the intrinsic fluorescence intensity of a ligand is measured as the ligand is released when the aptamer is thermally unfolded. First derivative analysis of the MN19•cocaine thermal shift provides a T_m value of 26.6 ± 0.8 °C while the OR3•cocaine complex has a T_m value of 31.0 ± 0.7 °C (Fig. 3). For the MN19•quinine thermal shift, a T_m value of 35.2 ± 0.3 °C was obtained, and for the OR3•quinine complex a T_m value of 44.6 ± 0.7 °C was measured.

3.2. Ligand binding analysis using ITC methods

The affinity for cocaine of the different stem 2 variants was gauged by ITC methods using a low-c binding method [27]. The affinity values of the different aptamer constructs are shown in Table 2. These data demonstrate that changing the sequence of stem 2 does not reduce the affinity of these aptamers for cocaine when compared with the affinity of MN19 for cocaine, and may be

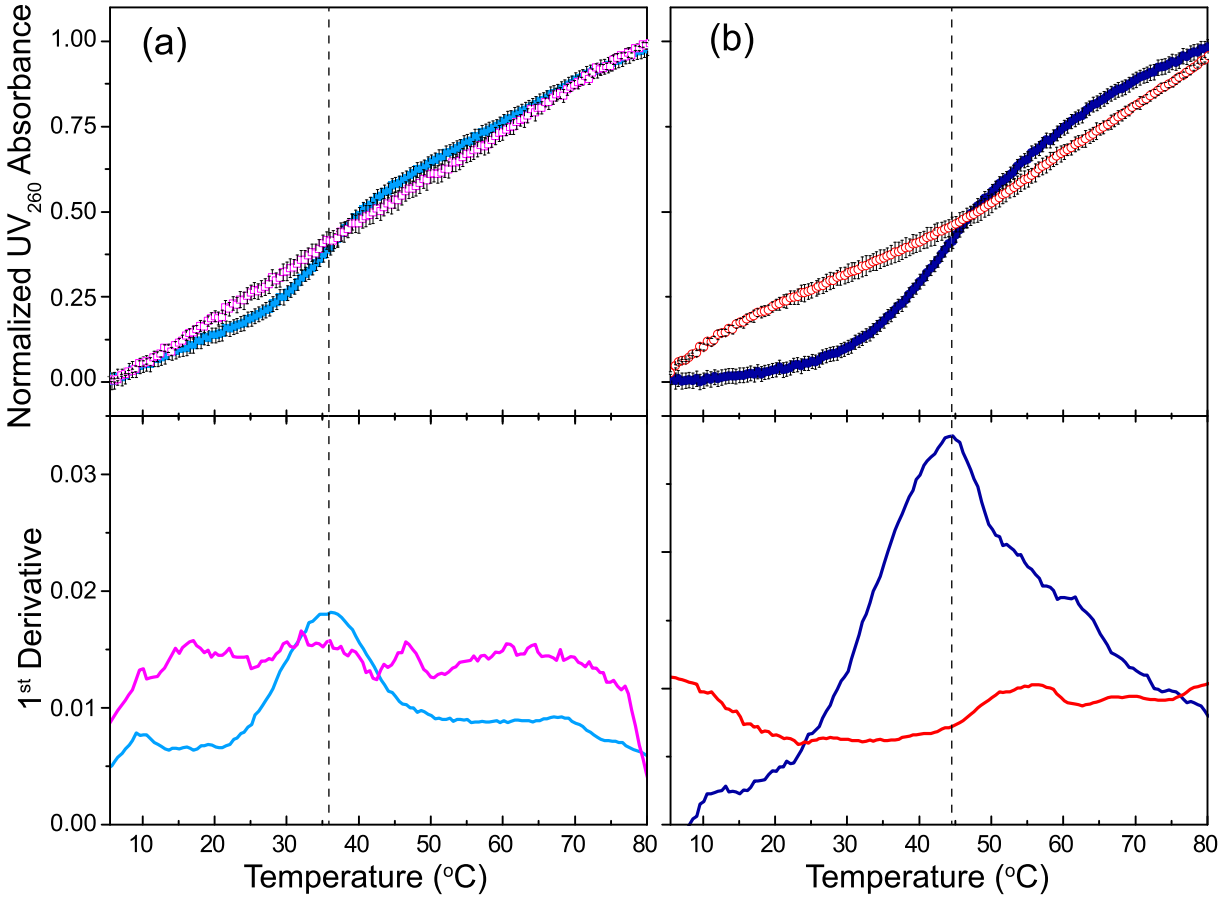

Fig. 2. Analysis of thermal stability using UV-monitored melting curves. Shown is the normalized UV absorbance at 260 nm for the (a) MN19 both free (open pink squares) and quinine-bound (filled blue squares) and (b) OR3 free (open red circles) and quinine-bound (filled blue circles). On top are the UV_{260} absorbance plots in a temperature range of 5 °C–80 °C. On the bottom, the first derivative of the melts are shown. Dashed lines designate the T_m point of aptamer-quinine complexes. Each data point denotes an average of 4–6 experiments with the error bars corresponding to one standard deviation. Data acquired in 20 mM sodium phosphate buffer (pH 7.4), 140 mM NaCl.

Table 1
Thermal denaturation temperature for aptamer-quinine complexes determined by UV melts.[a]

Aptamer	MN19	MN20	OR1	OR2	OR3
T_m (°C)	35.5 ± 0.3	40.2 ± 0.2	44.0 ± 0.2	43.7 ± 0.3	44.2 ± 0.1

[a] Data acquired in 20 mM sodium phosphate (pH 7.4), 140 mM NaCl. The values reported are averages of 4–6 individual experiments. The error range reported is one standard deviation.

considered marginally tighter.

The OR3 aptamer was then chosen for further ITC binding analysis by measuring its affinity to quinine at both high and low NaCl conditions with representative thermograms from these titrations shown in Fig. 4. At 140 mM NaCl concentration, OR3 bound quinine at a single-site with a K_d value of (0.73 ± 0.04) μM, a ΔH of (−22.5 ± 0.1) kcal mol^{-1} and a -TΔS value of (14.3 ± 0.4) kcal mol^{-1}. At the same experimental conditions, MN19 binds quinine at a single-site with a K_d value of (0.94 ± 0.04) μM, a ΔH of (−30.6 ± 0.2) kcal mol^{-1} and a -TΔS value of (22.5 ± 0.4) kcal mol^{-1}. With no added NaCl from the non-sigmoidal shape of the titrations curves (Fig. 4c and d), it is clear that both OR3 and MN19 bind quinine according to a two-independent site mechanism similar to what we observed previously [29]. At 20 °C, the temperature at which the high salt data was run, it is not possible to fit the 0 M NaCl data to the two-site model likely because binding at the second site is too weak resulting in too low a c-value to enable us to fit the data. When the data with no added NaCl was acquired at 15 °C (Fig. 4c and d) we were able to fit to a two independent site binding model [29]. The fit for MN19 binding quinine resulted in a K_{d1} of (0.25 ± 0.18) μM, a K_{d2} of (29 ± 6) μM, a ΔH_1 of (−28.0 ± 0.3) kcal mol^{-1}, a ΔH_2 of (−67 ± 14) kcal mol^{-1}, a $-T\Delta S_1$ value of (19 ± 13) kcal mol^{-1} and a $-T\Delta S_2$ value of (61 ± 18) kcal mol^{-1}. The fit for OR3 binding quinine resulted in a K_{d1} of (0.23 ± 0.13) μM and a K_{d2} of (75 ± 49) μM, a ΔH_1 of (−21.1 ± 0.2) kcal mol^{-1}, a ΔH_2 of (−19 ± 12) kcal mol^{-1}, a $-T\Delta S_1$ value of (12 ± 7) kcal mol^{-1} and a $-T\Delta S_2$ value of (14 ± 12) kcal mol^{-1}.

3.3. Structural analysis using NMR spectroscopy

NMR spectroscopy was used to analyse the structure and ligand binding ability of both the MN19 and OR3 aptamer constructs. In the ligand-free state, the OR3 aptamer shows imino peaks from 4 to 6 imino resonances indicative of a loosely or poorly structured ligand-free state (Fig. 5a). As cocaine is titrated into OR3, new imino signals appear in the NMR spectrum until the molecule is fully bound by cocaine. In the 1:1 OR3•cocaine, the expected number of signals is detected for the secondary structure shown in Fig. 1. For MN19, the NMR spectrum of the free aptamer shows 4–6 imino signals also indicative of a loosely or poorly structured ligand-free state (Fig. 5b). With the addition of cocaine, new imino signals appear, and in the 1:1 complex the expected number of signals are observed. Assignments shown in Fig. 5 for the 1:1 complex of OR3 were obtained from a comparison with those of MN19 [1].

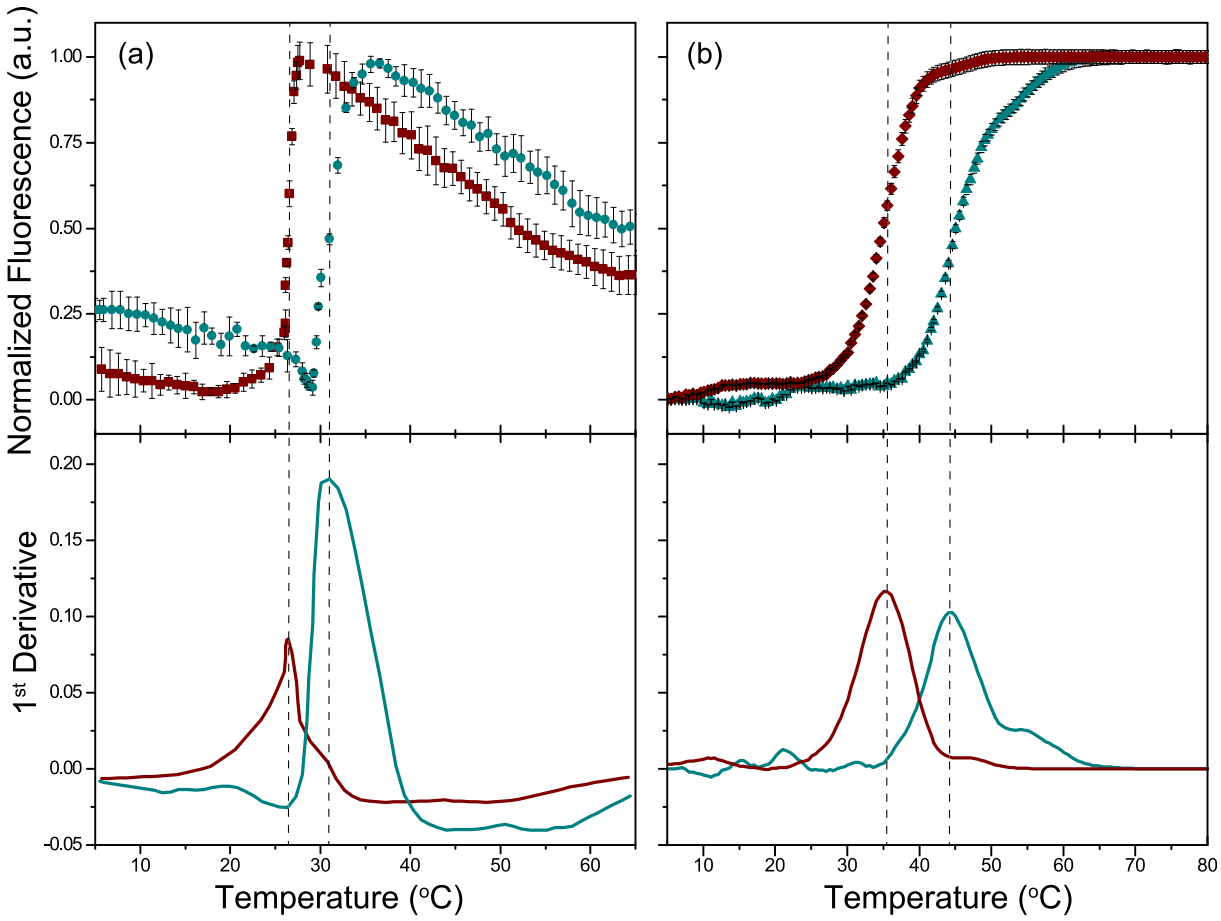

Fig. 3. Analysis of thermal stability using differential scanning fluorimetry thermal shift analysis. Displayed are the average intrinsic fluorescence responses for OR3-and MN19-ligand complexes. (a) On top is the MN19•cocaine complex (red) and OR3•cocaine (green) thermal shift assays. Cocaine is excited at 232 nm, and emission maxima detected at 320 nm in a temperature range of 5 °C–65 °C. (b) On top is the MN19•quinine complex (red) and OR3•quinine (green) thermal shift assays. Quinine is excited at 234 nm, and emission maxima detected at 383 nm in a temperature range of 5 °C–80 °C. On the bottom of each panel is the first derivative of the MN19•ligand and OR3•ligand thermal shifts. Dashed lines indicate the T_m point of each aptamer-ligand complex. Each data point denotes an average of 4–6 experiments with the error bars corresponding to one standard deviation. Data acquired in 20 mM sodium phosphate buffer (pH 7.4), 140 mM NaCl.

4. Discussion

At the start of this study, we wished to develop a thermal stable version of the cocaine-binding aptamer based on the rational design of its nucleotide sequence. The goals were: (1) to retain the ligand-induced structure-switching binding mechanism by retaining the three-base-pair stem 1 sequence; (2) to retain the ligand-binding affinity of the original MN19 sequence by not changing the nucleotides likely to be involved in interacting with the ligand (in stems 1 and 3, and at the three-way junction) as identified in our previous sequence variation and NMR-based chemical shift perturbation studies [1,4,37]; (3) to optimize the nucleotide sequence in stem 2 to increase the thermal stability of the bound aptamer. The results shown here demonstrate that we have achieved these goals.

As demonstrated by the imino NMR spectra of the OR3 aptamer, this molecule retains the ligand-induced structure switching mechanism of the original short stem 1 construct MN19 (Fig. 5). OR3 was chosen for structural analysis as it has the highest melt temperature of the aptamer-quinine complexes studied (Table 1). In the free state, the OR3 aptamer is loosely or poorly structured as demonstrated by its imino spectrum showing only 4–6 or the expected 11 signals. This behaviour is similar to other short stem 1 aptamers we have studied [1,4,26]. OR3 becomes structured as cocaine is titrated in and bound by the aptamer. The exact structural nature of the ligand-free short stem 1 aptamer state is not known. Small angle X-ray scattering (SAXS), a method that measures hydrodynamic parameters of molecules, shows that there is little change in the radius of gyration (R_g) or the maximum interatomic vector in the molecule (R_{max}) between free and ligand-bound MN19 [4]. As seen in the NMR spectra (Fig. 5), the fact that there are some imino signals present in the free state shows that some base pairs do form in stems 2 and 3 in the absence of ligand. The absence of some observable imino signals is possibly due to a high level of dynamics in the free state that is reduced with ligand binding. This reduction in dynamics is reflected in the reduction of the imino hydrogen exchange rates of both long and short stem 1 cocaine-binding aptamers upon ligand binding [5]. Whatever the nature of the structure of the free short stem 1 construct is, as demonstrated by the NMR spectra (Fig. 5), this nature is shared by both MN19 and OR3.

ITC methods were used to measure the ligand binding ability of the series of short stem 1 constructs studied here (Table 2). Previously, we demonstrated that the MN20 construct bound cocaine tighter than MN19 [37]. In the OR1, OR2 and OR3 constructs, the sequence changes used to optimize the thermal stability do not adversely affect cocaine binding, but result in a marginally tighter binding aptamer than MN19 (Table 2). Due to it having the highest

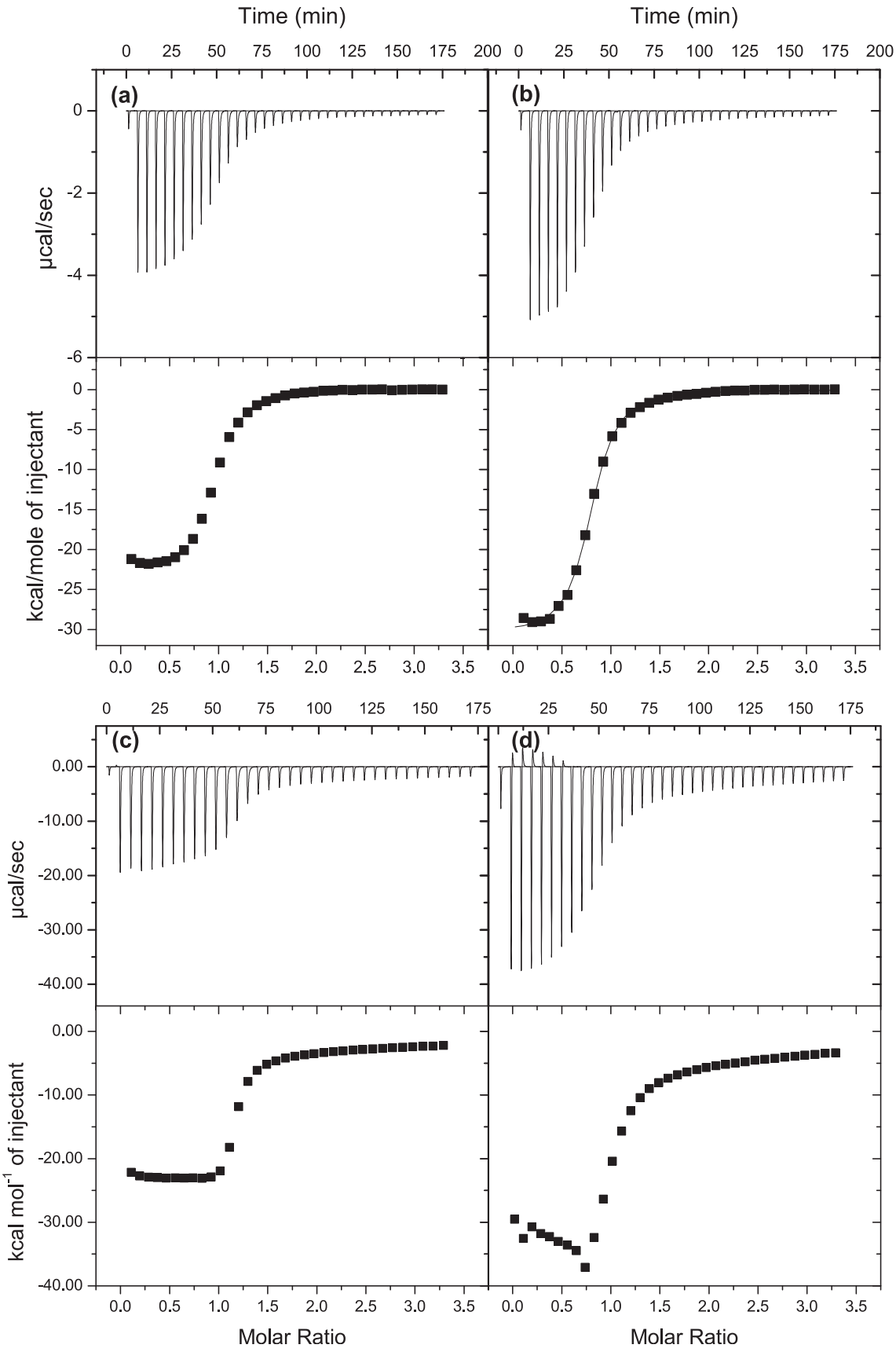

Fig. 4. Sample of ITC data showing the interaction of MN19 and OR3 with quinine. Data acquired in the presence of 140 mM NaCl results in single site binding with a K_d value of (0.73 ± 0.04) µM for (a) OR3 and a K_d value of (0.94 ± 0.04) µM for (b) MN19. Data acquired in the absence of added NaCl results in two-site binding for both (c) OR3 and (d) MN19. On top is the raw titration data showing the heat resulting from each injection of quinine into aptamer solution. On the bottom is the integrated heat plot after correcting for the heat of dilution. Both binding experiments were performed in a buffer of 20 mM TRIS (pH 7.4) at 20 °C (a & b) or 15 °C (c & d).

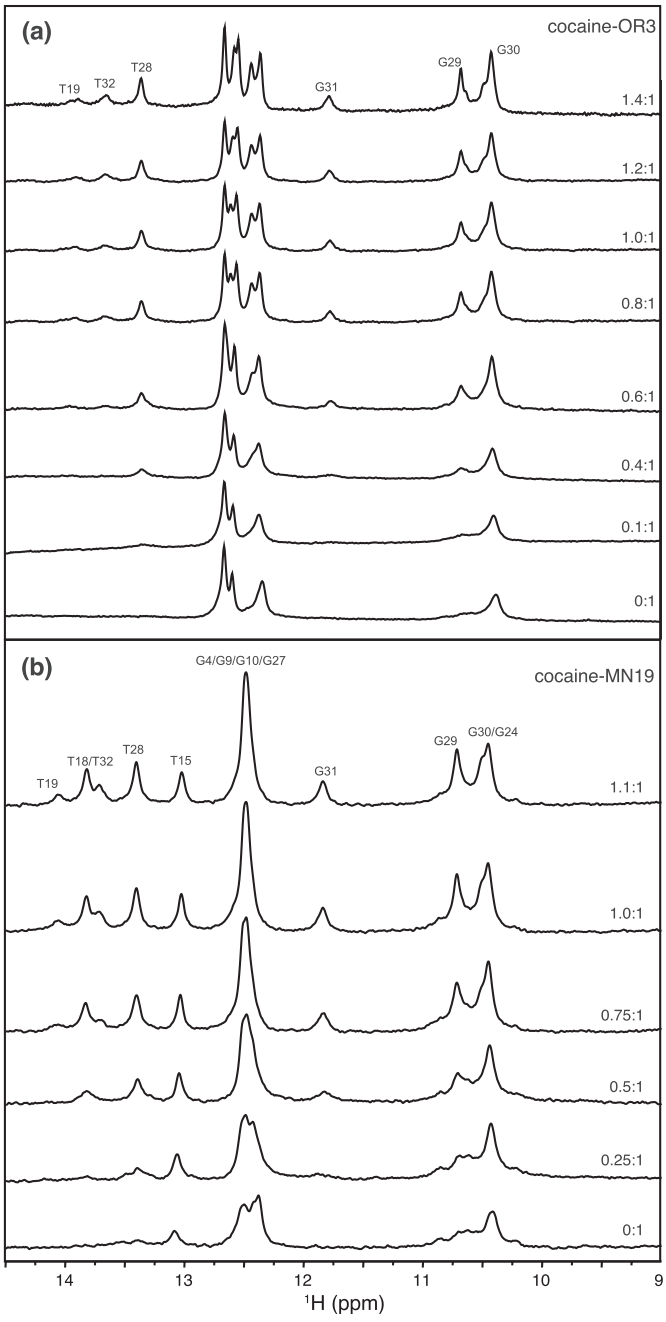

Fig. 5. Cocaine binding monitored by 1D ^{1}H-NMR. Displayed is the region of the NMR spectrum focusing on the imino resonances as a function of increasing cocaine concentration for (a) OR3 and (b) MN19. Note that for both of these aptamers, only a few peaks are observed in the free spectrum. Upon binding, sharp resonances resulting from the cocaine-bound aptamers appear. All spectra were acquired in 90% H_2O/10% $^{2}H_2O$ at 5 °C at the indicated molar ratio of cocaine to the corresponding aptamer.

thermal stability, OR3 was chosen for further ligand binding analyses using quinine as the ligand. Quinine binds the cocaine-binding aptamer ~50 fold tighter than cocaine [4,23,25,40], and this higher affinity makes it an ideal ligand for ITC analysis. The fits to the data in Fig. 4 shows that in high salt conditions OR3 binds quinine slightly tighter than MN19, mirroring the relative affinity seen for cocaine binding by these two aptamers (Table 2).

The sequence changes in stem 2 of OR3 coincide with the location of the NaCl concentration-dependant second (low affinity) ligand-binding site in the cocaine-binding aptamer [29]. We

Table 2
Binding affinity for the interaction between the different aptamer constructs and cocaine determined by ITC.[a]

Aptamer	MN19[b]	MN20[c]	OR1	OR2	OR3
K_d (μM)	26.7 ± 0.7	13 ± 7	24 ± 5	18.3 ± 0.8	21 ± 2

[a] Data acquired in 20 mM Tris (pH 7.4), 140 mM NaCl, 5 mM KCl at 20 °C. The values reported are averages of 3–4 individual experiments. The error range reported is one standard deviation.
[b] Data from Ref. [1].
[c] Data from Ref. [37].

therefore tested OR3 binding to quinine under buffer conditions of no added NaCl and determined that OR3 retains the ability to bind two molecules of quinine. In particular, the affinity of the high affinity site of MN19 and OR3 are identical within the error range but the affinity at the low-affinity site, the NaCl concentration-dependant site in stem 2 is significantly lower in OR3 than in MN19. When comparing the sequence of stem 2 in OR3 and MN19 we have retained the same number of Watson-Crick base pairs in both constructs though we have changed their identities. Retaining weak two-site binding in OR3 implies that binding at the second site depends at least to some extent on the shape of the aptamer but that the exact identity of the base pairs are needed for high affinity binding at this site.

The thermal stability of the structure-switching version of the cocaine-binding aptamer was optimized by changing the sequence in stem 2 to maximize ΔG according to the nearest neighbor thermodynamic parameters [41,42]. Additionally, the GAA triloop was shown to be the most stable DNA triloop sequence [43]. Simply changing the AT base pairs in MN19 to be GC base pairs, as in MN20, produced an increase in T_m value of 4.7 °C for the aptamer-quinine complex. By optimizing the sequence by staggering the GC base pairs, as in OR1, the T_m value of the aptamer-quinine complex increased to 44.0 °C. The final optimization step of replacing the AAA triloop with the more stable GAA triloop produced an improved T_m value for OR3•quinine to 44.2 °C. The increase in T_m values measured by UV melts was replicated using a differential scanning fluorimetry thermal shift assay (Fig. 3). The T_m values obtained in these assays for both MN19•quinine and OR3•quinine matched those found using UV melting experiments to within the experimental error. We think the OR3 construct will be useful for researchers using the cocaine-binding aptamer in biosensor development, as at room temperature (20–25 °C) a greater proportion of the aptamer-ligand complex will be folded using the OR3 sequence. Therefore, this should provide a more intense signal in an assay that depends on the structure-switching function of the aptamer.

The OR3 and MN19 aptamer constructs bound to cocaine were chosen for further stability analysis using the fluorescence-based thermal shift assay. Consistent with the lower binding affinity of MN19 and OR3 to cocaine than quinine, the MN19 and OR3 complexes with cocaine have a lower T_m value than their respective complexes with quinine. Additionally, as seen in the quinine complexes, the OR3-cocaine complex is more stable than the MN19-cocaine complex. Our proposed mechanism for what is occurring is that the sequence changes made in OR3 have stabilized either the ligand-free aptamer state, but not enough to produce a folded unbound aptamer, or has stabilized the ligand-bound folded state, with respect to MN19. If we assume that each ligand interacts with MN19 and OR3 with roughly the same ΔG value, less free energy from binding needs to go into folding the OR3 aptamer than the MN19 aptamer leaving more free energy to go into the observed binding free energy resulting in tighter binding observed for the OR3 aptamer and a higher melt temperature than we observe for

MN19.

In conclusion, we have developed a new cocaine-binding aptamer construct (OR3) that retains the ligand-induced structure-switching binding mechanism critical to biosensing applications, has a K_d value slightly tighter than the original MN19 aptamer, and has a significantly higher melt temperature when bound to both cocaine and quinine than observed for the original sequence. The more favorable thermal stability characteristics of the OR3 aptamer should make it a useful construct of the cocaine-binding aptamer in biosensing applications.

Acknowledgments

We thank Logan Donaldson (York University) for the use of his spectrofluorometer, Robert Harkness and Tony Mittermaier (McGill University) as well as past and present lab members for useful discussions. This work was supported by funding from the Natural Sciences and Engineering Research Council of Canada (NSERC) (grant number RGPIN-238562-2013) to P.E.J.

References

[1] M.A.D. Neves, O. Reinstein, P.E. Johnson, Defining a stem length-dependant binding mechanism for the cocaine-binding aptamer. A combined NMR and calorimetry study, Biochemistry 49 (2010) 8478–8487.
[2] M.N. Stojanovic, P. de Prada, D.W. Landry, Aptamer-based folding fluorescent sensor for cocaine, J. Am. Chem. Soc. 123 (2001) 4928–4931.
[3] P. Cekan, E.O. Jonsson, S.T. Sigurdsson, Folding of the cocaine aptamer studied by EPR and fluorescence spectroscopies using the bifunctional spectroscopic probe Ç, Nucleic Acids Res. 37 (2009) 3990–3995.
[4] O. Reinstein, M. Yoo, C. Han, T. Palmo, S.A. Beckham, M.C.J. Wilce, P.E. Johnson, Quinine binding by the cocaine-binding aptamer. Thermodynamic and hydrodynamic analysis of high-affinity binding of an off-target ligand, Biochemistry 52 (2013) 8652–8662.
[5] Z.R. Churcher, M.A.D. Neves, H.N. Hunter, P.E. Johnson, Comparison of the free and ligand-bound imino hydrogen exchange rates for the cocaine-binding aptamer, J. Biomol. NMR 68 (2017) 33–39.
[6] B.R. Baker, R.Y. Lai, M.S. Wood, E.H. Doctor, A.J. Heeger, K.W. Plaxco, An electronic, aptamer-based small-molecule sensor for the rapid, label-free detection of cocaine in adulterated samples and biological fluids, J. Am. Chem. Soc. 128 (2006) 3138–3139.
[7] T. Li, B. Li, S. Dong, Adaptive recognition of small molecules by nucleic acid aptamers through a label-free approach, Chem. - Eur. J. 13 (2007) 6718–6723.
[8] Y. Li, H. Qi, Y. Peng, J. Yang, C. Zhang, Electrogenerated chemiluminescence aptamer-based biosensor for the determination of cocaine, Electrochem. Commun. 9 (2007) 2571–2575.
[9] J. Chen, J. Jiang, X. Gao, G. Liu, G. Shen, G. Yu, A new aptameric biosensor for cocaine based on surace-enhanced raman scattering spectroscopy, Chem. - Eur. J. 14 (2008) 8374–8382.
[10] A.E. Abelow, O. Schepelina, R.J. White, A. Vallee-Belisle, K.W. Plaxco, I. Zharov, Biomimetic glass nanopores employing aptamer gates responsive to a small molecule, Chem. Commun. 46 (2010) 7984–7986.
[11] D. Tang, J. Tang, Q. Li, B. Su, G. Chen, Ultrasensitive aptamer-based multiplexed electrochemical detection by coupling distinguishable signal tags with catalytic recycling of DNase I, Anal. Chem. 83 (2011) 7255–7259.
[12] Z. Zhou, Y. Du, S. Dong, Double-strand DNA-templated formation of copper nanoparticles as fluorescent probe for label-free aptamer sensor, Anal. Chem. 83 (2011) 5122–5127.
[13] X. Hu, L. Mu, Q. Zhou, J. Wen, J. Pawliszyn, ssDNA aptamer-based column for simultaneous removal of nanogram per liter level of illicit and analgesic pharmaceuticals in drinking water, Environ. Sci. Technol. 45 (2011) 4890–4895.
[14] J. Das, K.B. Cederquist, A.A. Zaragoza, P.E. Lee, E.H. Sargent, S.O. Kelley, An ultrasensitive universal detector based on neutralizer displacement, Nat. Chem. 4 (2012) 642–648.
[15] J. Zhou, A.V. Ellis, H. Kobus, N.H. Voelcker, Aptamer sensor for cocaine using minor groove binder based energy transfer, Anal. Chim. Acta 719 (2012) 76–81.
[16] A. Porchetta, A. Vallee-Belisle, K.W. Plaxco, F. Ricci, Using distal-site mutations and allosteric inhibition to tune, extend, and narrow the useful dynamic range of aptamer-based sensors, J. Am. Chem. Soc. 134 (2012) 20601–20604.
[17] B. Malile, J.I. Chen, Morphology-based plasmonic nanoparticle sensors: controlling etching kinetics with target-responsive permeability gate, J. Am. Chem. Soc. 135 (2013) 16042–16045.
[18] G. Bozokalfa, H. Akbulut, B. Demir, E. Guler, Z.P. Gumus, D. Odaci Demirkol, E. Aldemir, S. Yamada, T. Endo, H. Coskunol, S. Timur, Y. Yagci, Polypeptide functional surface for the aptamer immobilization: electrochemical cocaine biosensing, Anal. Chem. 88 (2016) 4161–4167.
[19] F. Shahdost-fard, M. Roushani, Conformation switching of an aptamer based on cocaine enhancement on a surface of modified GCE, Talanta 154 (2016) 7–14.
[20] M.A.D. Neves, C. Blaszykowski, M. Thompson, Utilizing a key aptamer structure-switching mechanism for the ultrahigh frequency detection of cocaine, Anal. Chem. 88 (2016) 3098–3106.
[21] P. Dauphin-Ducharme, K.W. Plaxco, Maximizing the signal gain of electrochemical-DNA sensors, Anal. Chem. 88 (2016) 11654–11662.
[22] E. Guler, G. Bozokalfa, B. Demir, Z.P. Gumus, B. Guler, E. Aldemir, S. Timur, H. Coskunol, An aptamer folding-based sensory platform decorated with nanoparticles for simple cocaine testing, Drug Test. Anal. 9 (2017) 578–587.
[23] R. Pei, A. Shen, M.J. Olah, D. Stefanovic, T. Worgall, M.N. Stojanovic, High-resolution cross-reactive array for alkaloids, Chem. Commun. (2009) 3193–3195.
[24] J. Bao, S.M. Krylova, O. Reinstein, P.E. Johnson, S.N. Krylov, Label-free solution-based kinetic study of aptamer-small-molecule interactions reveals how kinetics control equilibrium, Anal. Chem. 83 (2011) 8387–8390.
[25] R.W. Harkness, S. Slavkovic, P.E. Johnson, A.K. Mittermaier, Rapid characterization of folding and binding interactions with thermolabile ligands by DSC, Chem. Commun. 52 (2016) 13471–13474.
[26] O. Reinstein, M.A.D. Neves, M. Saad, S.N. Boodram, S. Lombardo, S.A. Beckham, J. Brouwer, G.F. Audette, P. Groves, M.C.J. Wilce, P.E. Johnson, Engineering a structure switching mechanism into a steroid binding aptamer and hydrodynamic analysis of the ligand binding mechanism, Biochemistry 50 (2011) 9368–9376.
[27] J. Tellinghuisen, Isothermal titration calorimetry at very low c, Anal. Biochem. 373 (2008) 395–397.
[28] L.A. Freiburger, K. Auclair, A.K. Mittermaier, Elucidating protein binding mechanisms by variable-c ITC, ChemBioChem 10 (2009) 2871–2873.
[29] M.A.D. Neves, S. Slavkovic, Z.R. Churcher, P.E. Johnson, Salt-mediated two-site ligand binding by the cocaine-binding aptamer, Nucleic Acids Res. 45 (2017) 1041–1048.
[30] J.B. Murray, H.I. Al-Shora, Stability of cocaine in aqueous solution, J. Clin. Pharm. 3 (1978) 1–6.
[31] M. Van De Weert, Fluorescence quenching to study protein-ligand binding: common errors, J. Fluoresc. 20 (2010) 625–629.
[32] M. Van De Weert, L. Stella, Fluorescence quenching and ligand binding: a critical discussion of a popular methodology, J. Mol. Struct. 998 (2011) 145–150.
[33] F.H. Niesen, H. Berglund, M. Vedadi, The use of differential scanning fluorimetry to detect ligand interactions that promote protein stability, Nat. Protoc. 2 (2007) 2212–2221.
[34] S. Kiyonaka, T. Kajimoto, R. Sakaguchi, D. Shinmi, M. Omatsu-Kanbe, H. Matsuura, H. Imamura, T. Yoshizaki, I. Hamachi, T. Morii, Y. Mori, Genetically encoded fluorescent thermosensors visualize subcellular thermoregulation in living cells, Nat. Methods 10 (2013) 1232–1238.
[35] F. Vollrath, N. Hawkins, D. Porter, C. Holland, M. Boulet-Audet, Differential Scanning Fluorimetry provides high throughput data on silk protein transitions, Sci. Rep. 4 (2014) 5625.
[36] H.S.P. Rao, A. Desai, I. Sarkar, M. Mohapatra, A.K. Mishra, Photophysical behavior of a new cholesterol attached coumarin derivative and fluorescence spectroscopic studies on its interaction with bile salt systems and lipid bilayer membranes, Phys. Chem. Chem. Phys. 16 (2014) 1247–1256.
[37] M.A.D. Neves, O. Reinstein, M. Saad, P.E. Johnson, Defining the secondary structural requirements of a cocaine-binding aptamer by a thermodynamic and mutation study, Biophys. Chem. 153 (2010) 9–16.
[38] M. Piotto, V. Saudek, V. Sklenar, Gradient-tailored excitation for single-quantum NMR spectroscopy of aqueous solutions, J. Biomol. NMR 2 (1992) 661–665.
[39] A.A. Shoara, S. Slavkovic, L.W. Donaldson, P.E. Johnson, Analysis of the interaction between the cocaine-binding aptamer and its ligands using fluorescence spectroscopy, Can. J. Chem. (2017), http://dx.doi.org/10.1139/cjc-2017-0380.
[40] S. Slavkovic, M. Altunisik, O. Reinstein, P.E. Johnson, Structure-affinity relationship of the cocaine-binding aptamer with quinine derivatives, Bioorg. Med. Chem. 23 (2015) 2593–2597.
[41] H.T. Allawi, J. SantaLucia Jr., Thermodynamics and NMR of internal G T mismatches in DNA, Biochemistry 36 (1997) 10581–10594.
[42] J. SantaLucia Jr., D. Hicks, The thermodynamics of DNA structural motifs, Annu. Rev. Biophys. Biomol. Struct. 33 (2004) 415–440.
[43] S. Yoshizawa, G. Kawai, K. Watanabe, K.-i. Miura, I. Hirao, GNA trinucleotide loop sequences producing extraordinarily stable DNA minihairpins, Biochemistry 36 (1997) 4761–4767.